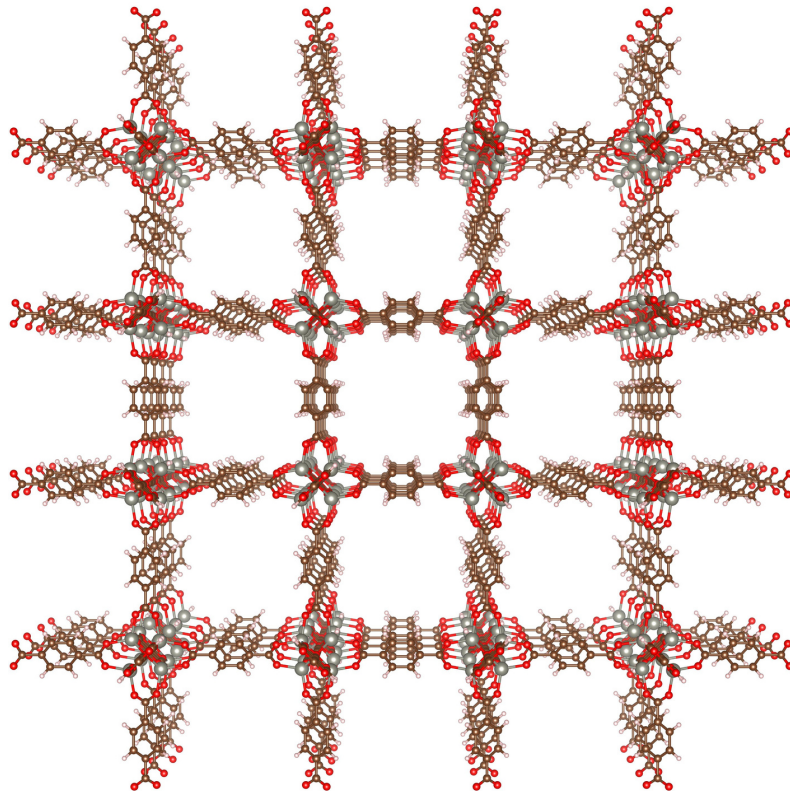


Volume 10, Issue 1, June 2023

ISSN 2542-2545

The
**HIMALAYAN
PHYSICS**

A peer-reviewed Journal of Physics



*Department of Physics, Prithvi Narayan Campus, Pokhara
Nepal Physical Society, Gandaki Chapter, Pokhara*

Publisher

*Department of Physics, Prithvinarayan Campus, Pokhara
Nepal Physical Society, Gandaki Chapter, Pokhara*

The Himalayan Physics

Volume 10, Issue 1, June 2023

ISSN 2542-2545

The Himalayan Physics (HimPhys) is an open access peer-reviewed journal that publishes quality articles which make innovative contributions in all areas of Physics. HimPhys is published annually by Nepal Physical Society (Gandaki Chapter), and Department of Physics, Prithvi Narayan Campus, Pokhara. The goal of this journal is to bring together researchers and practitioners from academia in Nepal and abroad to focus on advanced techniques and explore new avenues in all areas of physical sciences and establishing new collaborations with physics community in Nepal.

Chief Editor

Aabiskar Bhusal

©2023, Publishers. All rights reserved.

This publication is in copyright. Subject to statutory exception and to the provisions of relevant collective licensing agreements, no reproduction of any part may take place without written permission of the publishers.

Cover: Ball-and-stick model of MOF-5. © Roshani Sharma. Printed with permission.

Volume 10, Issue 1, June 2023

ISSN 2542-2545

The
**HIMALAYAN
PHYSICS**

A peer-reviewed Journal of Physics

Chief Editor

Aabiskar Bhusal

Publisher

*Department of Physics, Prithvi Narayan Campus, Pokhara
Nepal Physical Society, Gandaki Chapter, Pokhara*

Nepal Physical Society

Gandaki Chapter

Pokhara, Nepal

President

Dr. Krishna Raj Adhikari

Immediate Past President

Min Raj Lamsal

Vice-President

Dr. Kapil Adhikari

Secretary

Ravi Karki

Treasurer

Dipak Adhikari

Joint Secretary

Amrit Dhakal

Editorial Member

Aabiskar Bhusal

Members

Bhuban Subedi

Man Bahadur Roka

Sabin Gautam

Sristi Gurung

Suresh Poudel

Advisory Board

Pabitra Mani Poudyal

Surya Bahadur G.C.

Parashu Ram Poudel

Jeevan Regmi

Kul Prasad Dahal

Himalayan Physics Vol-10(1) (2023)

TABLE OF CONTENTS

Adsorption of toxic gases by metal-organic frameworks D. Adhikari, R. Karki, K. Adhikari, N. Pantha	1
Cluster modelling of MOF-5 and its application on gas storage R. Sharma, S. Gurung, K. Adhikari	25
Electronic and magnetic properties of ternary sulfide $Rb_2Mn_3S_4$ G.B. Acharya, M.P. Ghimire	33
Dust properties around NGC 7023 nebula in interstellar medium using IRIS, AKARI, and WISE survey A. Subedi, A. Chaudhary, K. Chaudhary, K. Khatiwada, R. Kandel, S. N. Yadav, D. R. Upadhyay, A. K. Jha	40
Experimental design for tri-state logic H.S. Mallik, R. Rijal, H.P. Lamichhane	51
Comparison of aerosol optical properties over Lumbini, Pokhara and Langtang-Base Camp S. Sapkota, S. Gautam, A. Gautam, R. Poudel, S. Pokheral, K. Basnet, A. Subedi	58
Wavelet coherence analysis foF2 over Boulder station during different geomagnetic activity A. Giri, B. Adhikari, B. Shrestha, S. Rimal	66
Complex impedance analysis of soft chemical synthesized NZCF systems D. Parajuli, V.K. Vagolu, K. Chandramoli, N. Murali, B.R. Sharma, N.L. Shah, K. Samatha	78
Controlling pests in post-harvested wheat using microwave heating H.B. Pariyar, S. Dhungana, D.R. Paudel	86
Mean value and velocity variation of ions in different magnetic field at constant obliqueness B.R. Adhikari	99
Comparative study of solar flux using different empirical models at low land urban industrial zone of Biratnagar Nepal F. Limbu, B.R. Tiwari, U. Joshi, J. Regmi, I.B. Karki, K.N. Poudyal	100

Wavelet coherence analysis of foF2 over Boulder station during different geomagnetic activity

Research Article

Ashutosh Giri¹, Binod Adhikari^{1,2*}, Bikas Shrestha¹, Shramik Rimal¹

1 Department of Physics, St. Xavier's College, Tribhuvan University, Kathmandu, Nepal.

2 Department of Physics, Patan Multiple College, Tribhuvan University, Nepal.

Abstract: A geomagnetic storm is a major disturbance of Earth's magnetosphere that occurs when there is a very efficient exchange of energy from the solar wind into the space environment surrounding Earth. During solar and geomagnetic activities, critical frequency of F2 layer (foF2) varies in a great extent. The focus of the current study is on variations in foF2, the critical frequency of the F2 layer, during the intense geomagnetic storm of solar cycle 24 and quiet storm of solar cycle 25. The foF2 data of mid latitude station BC840 (Boulder) in the American region have been used to study geomagnetic and solar wind properties linked with foF2. Time series analysis and Wavelet Coherence analysis have been used to establish the relationship between those parameters. We have found considerable effect of solar and geomagnetic storm disturbances on foF2 during the geomagnetic storm time. The foF2 is enhanced prior to the storm and depletes during recovery phase with no significant changes observed during weak storm. The enhancement or depletion in foF2 may be used as precursor of geomagnetic storms. With long trend analysis and larger database we can make a catalog which can be used to predict the geomagnetic storm and deepen our understanding in impacts of storms on communication signals due to energy injected in ionosphere.

Keywords: Geomagnetic storm • Coronal mass ejection (CME) • Ionosphere • Critical frequency of F2 layer (foF2) • Wavelength coherence (WTC)

I. Introduction

The daily and yearly changes in the ionospheric F2 area follow typical patterns. These patterns vary significantly from day to day. Still, when energy from the solar wind is injected into the polar ionosphere during geomagnetic storms, remarkable shifts (positive or negative anomalies) take place [1]. Changes in the thermosphere's composition, temperature, and circulation impact the F2 region's electron concentration and the movement of hot gas from polar to lower latitudes. Further, Ionospheric currents, currents carried by magnetospheric boundaries such as the magnetopause or ionopause, magnetotail currents, and currents flowing inside magnetospheres such as ring currents, plasma sheet currents, and currents aligned to magnetic field lines (or field-aligned currents) are among the many types of current systems produced by planets' interactions with the solar wind [2]. One of the most important and unresolved problems in ionospheric physics is how the ionosphere's Total Electron Content

* Corresponding Author: binod.adhi@gmail.com

(TEC) and F region react to geomagnetic storms [3–9]. Different numerical models of the ionosphere have been used in theoretical studies [10–14], as well as more intricate models of the Earth’s upper atmosphere [15–19]. These investigations deepen our understanding of ionospheric reactions to geomagnetic storms. The mechanisms underlying the positive ionospheric storm development in the ionospheric F zone remain poorly understood, despite clear advances in this avenue of research. The strengthening of the high-latitude ionospheric electric fields, currents, and auroral particle precipitation causes the thermosphere to heat up during geomagnetic storms. This heating causes the more neutral wind to blow toward the equator [3]. According to several studies [4, 20], the equatorward neutral wind transports plasma upward along the inclined geomagnetic field lines at low and mid-latitudes into the regions with lower chemical loss rates in ion-molecular reactions. This causes an increase in F region electron density.

Fast Coronal Mass Ejections’ (CMEs’) are the main interplanetary phenomena during solar maximum that trigger powerful magnetic storms. The sheath region immediately follows the forward shock, and the CME ejects itself in two interplanetary structures crucial for generating storms featuring strong southbound Interplanetary Magnetic Fields (IMFs). The major phase of a storm is generated by southerly IMFs, as opposed to the initial phase, which is brought on by an increase in plasma pressure brought on by an increase in density and speed at and behind the shock followed by a Sudden Impulse (SI) at Earth. Two-step main phase storms with larger storm intensities may develop if the fields are southerly in both the sheath and solar ejecta. With delays of 1-2 hours, the storm recovery phase starts when the IMF moves less southward. It normally lasts 10 hours before it decays. The strength of the core magnetic field and the amplitude of the cloud speed appear to be correlated for CMEs involving clouds, with a tendency that faster-moving clouds tend to have stronger core magnetic field strengths, both of which contribute to the development of intense storms because those two parameters are crucial in producing the solar wind-magnetosphere coupling through the reconnection process [21].

Dessler & Parker [22] and Scokpe [23] showed that the ring current and Disturbance storm time (Dst) index reduced the equatorial magnetic field power that is proportional to the total energy of the ring current particles. It’s a reliable indicator of the energetics of the magnetic storm. The strength of the ring current is measured in terms of the Dst index, with contributions from the magnetopause current. Dst index helps to create a database for solar ejecta and provides information on the growth of the solar electrojet and the frequency of solar flares. It assists in identifying both the frequency and potential causes of solar and planetary events [24]. Gonzalez [25] measured the energy emitted during the geomagnetic superstorm’s primary phase. They found that during the primary phase of geomagnetic storms, 1 to 4 per cent of the energy present in the solar wind gets transported to the magnetosphere. The majority of transmitted energy roughly 25 to 40 per cent is pushed into the ring current, with the remaining 16 to 24 per cent dissipating into the auroral ionosphere.

II. Dataset and Methodology

In this research, the ionosonde data for foF2 layer critical frequency were provided by Global Ionospheric Radio Observatory (GIRO) that is hosting the Digital Ionogram Database (DIDB), available via <https://giro.uml.edu/didbase/scaled.php> (accessed on 31 March, 2022). The resampling interval of ionosonde stations is of 5 minutes for 5 days. The selected station is BC840 (Boulder 40.0150° N, 105.2705° W). The space weather data measured during 2 geomagnetic storms of the solar cycle 24 and 25 is provided by the Omni web data source which is maintained by the Space Physics Data Facility of NASA/Goddard Space Flight Centre (https://omniweb.gsfc.nasa.gov/form/omni_min.html). These events were selected based on the Dst index derived from a network of near-equatorial geomagnetic observatories. From the OMNI system, we selected data observation for velocity along the z direction (Vz), Flow speed (Vsw), Temperature (Tsw), Symmetric Horizontal Component of the geomagnetic field (SYM-H), Flow pressure (nPa), Electric field (Ey), Proton Density (Nsw), Component of an interplanetary magnetic field along the z-axis (IMF-Bz), and Asymmetric Horizontal Component of the geomagnetic field (ASY-H).

This work analyses our data using discrete time series analysis and Wavelet Coherence (WTC). Time series analysis is frequently applied to real-world atmosphere obtained from routine observations performed in two domains, i.e., frequency domain and time domain. This study's main motivating factors for time series analysis are pattern recognition, interruption detection, and forecasting of foF2 and other solar parameters.

Further, for concrete relation between foF2 and solar parameters, the Wavelet technique (WT) is imposed. WT is a collection of analytical tools that resolves time series into frequency, resembling two-time series in terms of frequency [26]. In time-frequency space, wavelet analysis is a strong tool for analyzing nonstationary signals and the localized oscillatory characteristic [27, 28]. Continuous Wavelet Transform (CWT) and Discrete Wavelet Transform (DWT) are the two types of WT. Because of its appropriate time and frequency localization, the Morlet wavelet (dimensionless frequency, $\omega_o = 6$) is an ideal option for extracting features [28]. The wavelet transform has been expanded to include the Cross Wavelet (XWT) and Wavelet Coherence (WTC), which are nonlinear algorithms for examining the phase connection between two-time series in the time-frequency domain [27, 28]. The WTC spectrum quantifies the degree to which two-time series co-vary as a function of time and frequency. The XWT spectrum exposes large shared power areas and relative phases between two-time series in time frequency space [29, 30]. The XWT of two-time series $X(t)$ and $Y(t)$ is defined as:

$$W_t^{XY}(s) = W_t^X(s)W_t^{Y*}(s) \quad (1)$$

The CWT coefficients of sequences $X(t)$ and $Y(t)$ at frequency scale s are denoted by $W_t^X(s)$, and $W_t^{Y*}(s)$ respectively and $*$ denotes the complex conjugate. $W_t^{XY}(s)$ produces a complicated result. Therefore, the modulus $W_t^{XY}(s)$ denotes regions of high specific power in time-frequency space. Because the wavelet powers are not normalized in XWT, Maraun, and Kurths [31] found that the XWT might give major misleading findings, i.e., the

spectrum of one of the time series shows large peaks although the two-time series have no link. To overcome this issue, wavelet coherence (WTC), a normalized measure for the connection between $X(t)$ and $Y(t)$, was developed, in which the XWT power is normalized by the spectrum of the two-time series

$$R_s(t) = \frac{w_t^{XY}(s)}{\sqrt{(W_t^X(s)W_t^{Y*}(s))}} \quad (2)$$

One can notice that the nominator and denominator of $R_s(t)$, the formulation can be equal if the spectrum is not calculated independently. As a result, some smoothing on the estimation of single and cross wavelet spectrums should be done in advance to estimate wavelet coherence [27], as follows:

$$R_t^2(s) = \frac{|S[s^{-1}W_t^{XY}(s)]|^2}{S[s^{-1}W_t^X(s)][s^{-1}W_t^Y(s)]} \quad (3)$$

Here, S is the smoothing operator and is given by [28];

$$S(W) = S_{\text{scale}} \left(S_{\text{time}} \left(W_t^{XY}(s) \right) \right)$$

Where, S_{scale} and S_{time} denote the smoothing along the wavelet scale axis and smoothing in time, respectively [27, 28, 31]. WTC values around 1 indicate a higher degree of resemblance across time series, whilst coherence values near 0 indicate no correlation.

In general, XWT can better expose common high-power time-frequency areas. At the same time, WTC is a powerful statistical tool for scrutinizing two-time series nonlinear behavior and determining significant coherence despite low common powers [31]. This work uses WTC analysis to determine the local correlation between two-time series in time-frequency space.

III. Results and Discussion

During geomagnetic storms, the earth's magnetic field is disrupted. The sun and the magnetosphere are linked, resulting in several changes that occurs both in interplanetary space and terrestrial environment on the ground [32]. Further, changes in magnetospheres causes change in ionosphere and its layers. This section presents the time series analysis of critical frequency of F2 layer, solar parameters, and geomagnetic indices during solar storms of 15-19th March, 2015 and quiet day of 25-29th January, 2022.

Event 1: 15-19 March, 2015

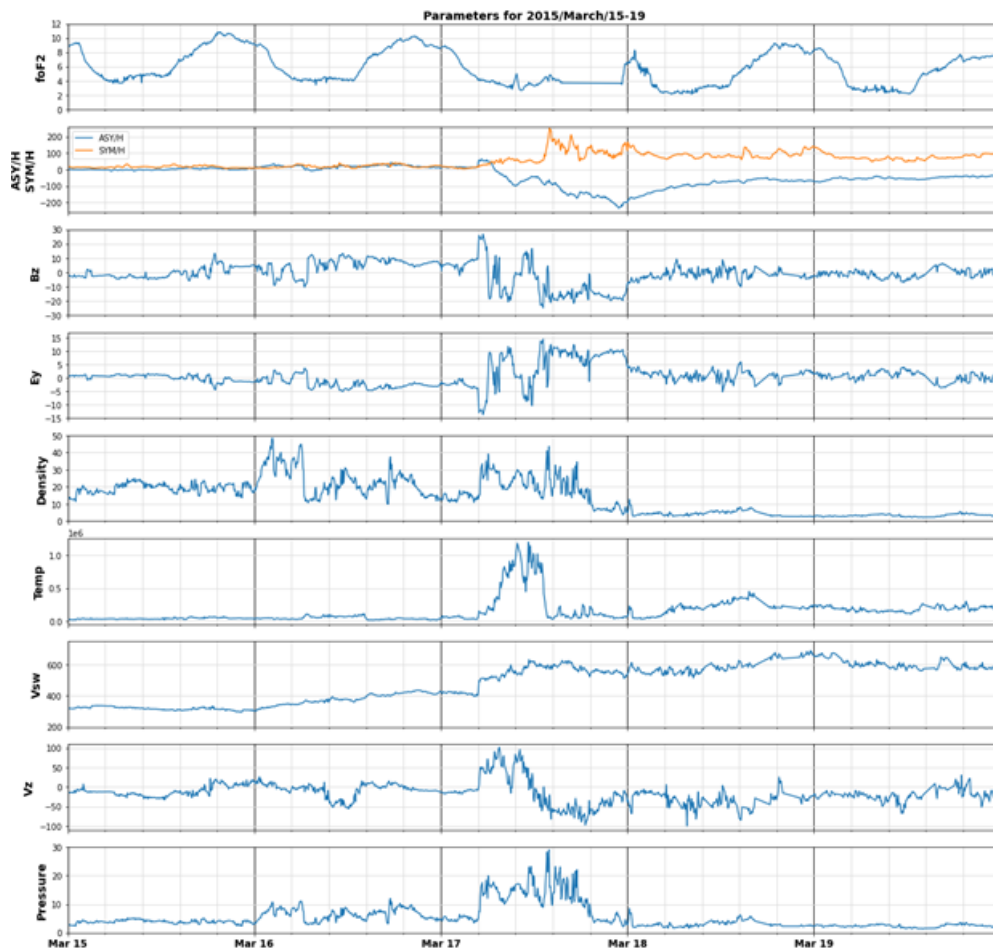


Figure 1. Critical frequency of F2 layer and geomagnetic indices during the storm of 17th March 2015. From top panel to bottom panel, top panel-Critical frequency of F2 layer (foF2, MHz), second panel- SYMH and ASYH (nT), third panel - IMF-Bz (nT), fourth panel-Electric field (E_y) (mV/m), fifth panel-Density (n/cc), sixth panel-Temperature (K), seventh panel-solar wind velocity (km/sec), eighth panel-velocity along z-direction (km/s) and ninth panel-flow pressure (nPa)

The first panel of Fig. 1 represents the value of foF2 for event 1, which shows a decrease in the frequency value at the start of the main event day of March 17, St. Patrick's Day. This negative geomagnetic storm response could be due to downward ExB drift (i.e. hmF2 depletion) and O/N2 depletion across the observatory region. Soon after the storm ends, we can see that the value of foF2 follows its normal trend, which validates the result of Klimenko et al. [19]. In the second and third panels, the storm began in the early hours of March 17 when the value of IMF-Bz turned southwards in the early hours. The value of SYM/H started to show decreasing effect. It reached the negative value of -200 nT. The value of IMF again turned northwards and again southwards during 10:00 LT, after which ASY/H started to increase, reaching the maximum value of 250 nT. The fourth panel shows the variation in Electric field strength. The value of the electric field strength can be seen reaching the minimum value of $\sim 14 \text{ mVm}^{-1}$ during the start of the event day and reaching the maximum value at 15:00 LT of the event day. On the other hand, the density on the fifth panel shows reaching a maximum of 50 n/cc a few hours before the storm's initiation and drops to the lowest value of $\sim 4 \text{ n/cc}$ during the recovery phase. The temperature shows an abrupt increase in value, reaching a maximum of $14 \times 10^6 \text{ K}$ during the storm time of March 17, following previous research works. In the seventh and eighth panels, we can see the value of solar wind velocity increasing abruptly during the early hours of March 17 as the storm turns southward and increases, suggesting Corotating Interaction Region (CIR) driven storm. And the vertical component of solar wind velocity can increase at first and then decrease as the storm continues. In the last panel, we can observe that the pressure increased significantly when the storm started.

Similarly, Fig. III describes the disparity of parameters for the weak storm of 2022, January 25-29. The first panel shows the vacillation of foF2, which shows a periodic variation of foF2 compared to event one, where there was a negative effect on foF2, suggesting foF2 might be used as a precursor of geomagnetic storms induced by CMEs. In the second and third panels, we studied the variation of ASY/H and SYM/H, which showed clear results for weak storm days. The value of SYM/H reached $\sim 5 \text{ nT}$ for January 26-28 from a high value of 80 nT on January 25. The value of ASY/H was also around -35 nT for the whole event day. This shows that the values are opposing the values of the event one day. We can also see that the value of Bz has no significant changes in the event of two days. The values lie in the range of (-10,10) nT for the quiet days. In the fourth panel, we can see that the electric field strength value also shows no significant variation remaining in the range of (-30, 5.0) mVm^{-1} compared to the storm day (-15, 15) mVm^{-1} is very low. In the fifth panel, we studied the variation of density, which shows a very low variation (0-10) n/cc compared to the storm days (0-50) n/cc. Also, in the next four panels, we can see no significant changes in the value of temperature, the velocity of the solar wind, and pressure in the quiet days compared to the storm days.

Event 2: 25-29 January, 2022

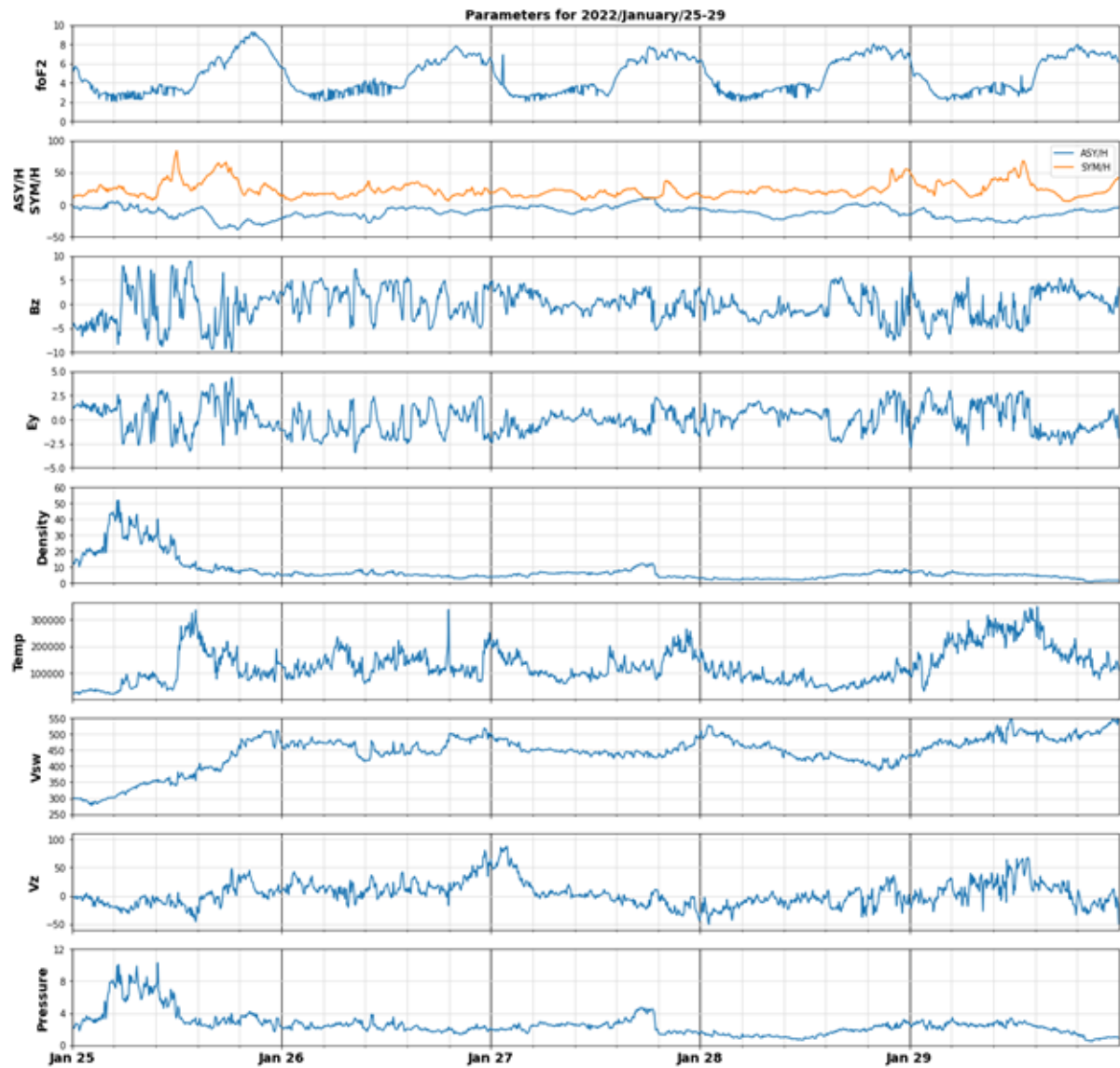


Figure 2. Critical frequency of F2 layer and geomagnetic indices during the storm of 27th January 2022. From top panel to bottom panel, top panel - Critical frequency of F2 layer (foF2, MHz), second panel-SYMH and ASYH (nT), third panel - IMF-Bz (nT), fourth panel - Electric field (E_y) (mV/m), fifth panel - Density (n/cc), sixth panel - Temperature (K), seventh panel - solar wind velocity (km/sec), eighth panel - Velocity along z-direction (km/s) and ninth panel - Flow pressure (nPa).

Wavelet Coherence (WTC) analysis

As discussed in the earlier section, the Fig. 3 clearly shows that all 8 parameters are correlated with foF2 at a periodicity of 64 minutes with very less COI. Still, V_z leads with a phase angle of nearly 90° , early on March 17th, our main event day. Again, there is a correlation between foF2 and Bz around the end of March 17th,

but here, foF2 and Vz are in the same phase. This is due to daytime and night-time behaviour. Similarly, foF2 and Vsw are strongly correlated in periodicity 64-128 minutes from March 17 to the end of March 18, with Vsw leading foF2 with some angle. No considerable COI can be seen in the case of other parameters.

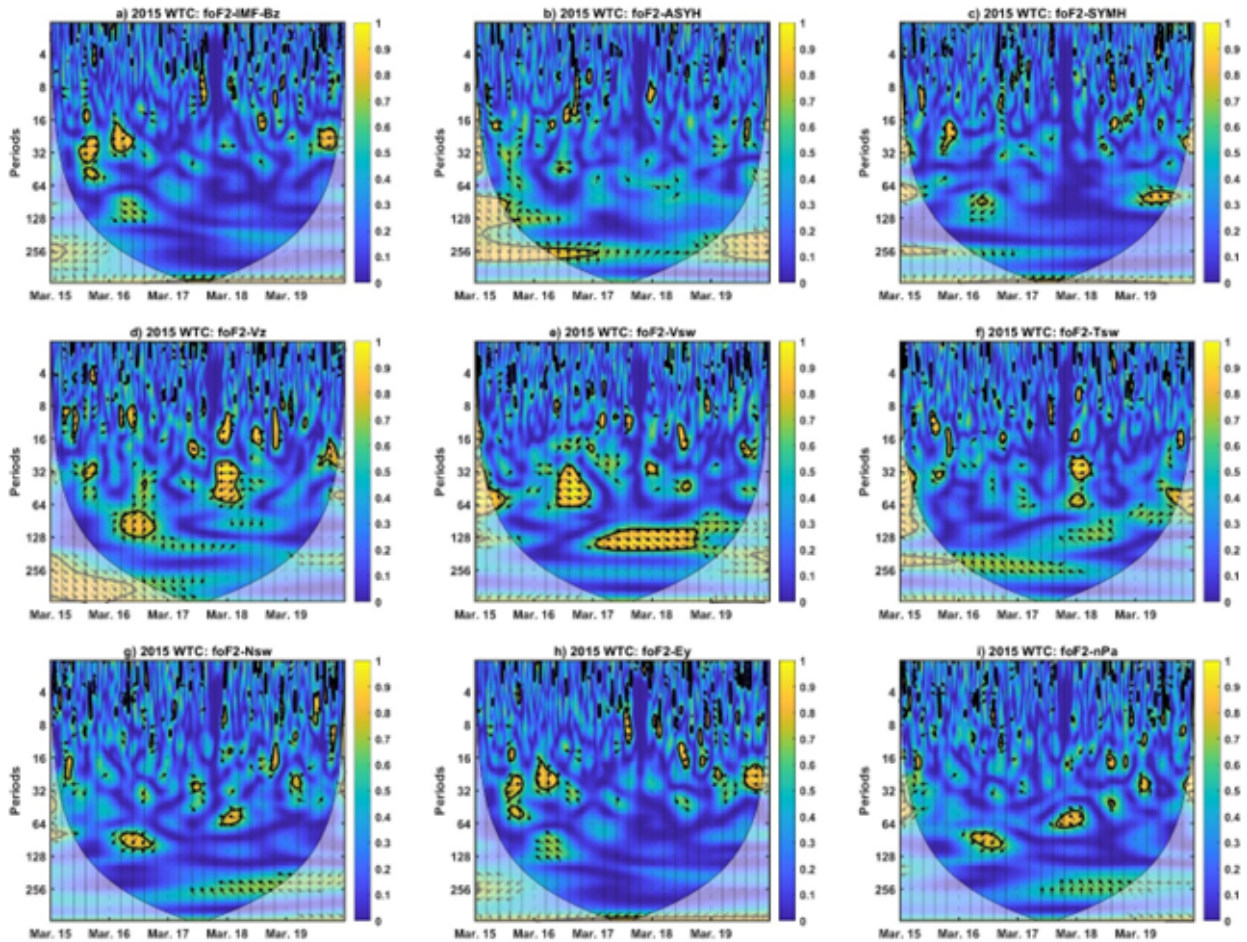


Figure 3. Wavelet scalogram of foF2 with Vz, Vsw and Temperature in first panel, SYM/H, nPa and Ev in second panel and Nsw, IMF-Bz and ASYH in bottom panel for geomagnetic storms of 2015 March 15-19

Similarly, from Fig. 4, we can clearly see that COI between foF2 and Vz, Vsw, and temperature aren't considerable in this event. However, a relation between SYM/H and foF2 can be seen before the event day. SYM/H is leading foF2 because of southward wind validating the results of Atulkar et al. [33]. Regarding flow pressure and proton density, we can observe COI at a periodicity of 70 minutes with the same phase for event day. In the case of ASY/H, which should be opposite to SYM/H. Here, no such relation can be seen if we consider foF2 as connecting link between SYM/H and ASY/H. This verifies the results that foF2 is affected by the southward wind, which validates the results of Pandit et al. [34].

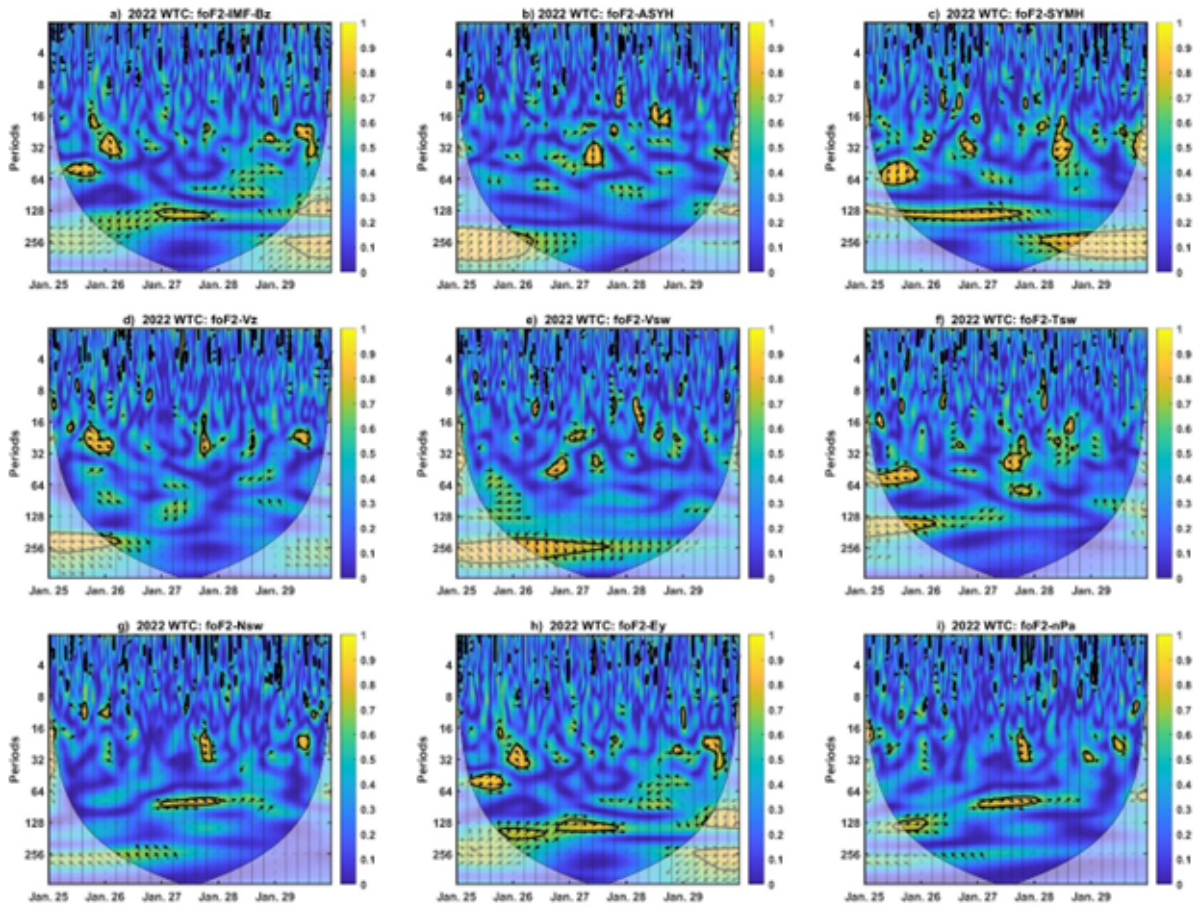


Figure 4. Wavelet scalogram of foF2 with V_z , V_{sw} and Temperature in first panel, SYM/H, nPa and E_v in second panel and N_{sw} , IMF-Bz and ASYH in bottom panel for geomagnetic storms of 2022 January 25-29

IV. Conclusions

The ionosphere's reaction to various levels of magnetic disturbances can be understood by analyzing foF2 at various geomagnetic activity levels. The ionosphere can become disturbed during geomagnetic activity, changing the electron density profiles and affecting radio wave transmission. The above work presents the deviation of the critical ionospheric frequency (foF2) variations for each storm event: 2015, March 17th and 2022, and January 27th at BC840 (Boulder 40.0150°N, 105.2705°W). The following conclusions can be drawn from our work:

- The foF2 depletion was observed for the station, validating the results of previous research, foF2 value can be seen as having a negative impact during the storm period and is seen to be having the same periodic variation as before the storm in the recovery period.
- During the quiet January 2022, no effect on the periodic value of foF2 was observed. The negative geomagnetic storm response could be due to downward $E \times B$ drift (i.e. hmF2 depletion) and O/N_2 depletion across the observatory region.

- The dependence of the storm time variation on the local time and the penetration of high latitude stations in the auroral region may be a better mechanism explaining the foF2 variations.
- WTC results show a strong dependence of dynamics of the foF2 layer on solar wind velocity with the same phase. During the recovery phase of both storms, there is depletion in the foF2 layer.

So we can conclude that the foF2 is enhanced before the storm and depletes during the recovery phase with no significant changes observed during the weak storm. WTC results show that the dynamics of the foF2 layer have a strong dependence on solar wind velocity with the same phase. As the storm days and ionospheric station utilized for this assertion are fairly restricted, it needs to be investigated further using a bigger database, implying that the critical frequency, and therefore the electron density, cannot be very localized. These findings may have significant implications for ionosphere-dependent communication and navigation systems, such as HF radio communications and GNSS positioning. We can foresee and lessen the impact of space weather on these systems by understanding how the ionosphere reacts to various amounts of geomagnetic activity.

V. Acknowledgements

The author would like to acknowledge the space weather data archive of the Low Resolution OMNI (LRO) of NASA, https://omniweb.gsfc.nasa.gov/form/omni_min.html and Global Ionospheric Radio Observatory (GIRO) that is hosting the Digital Ionogram Database (DIDB).

References

- [1] Danilov A. F2-region response to geomagnetic disturbances. *Journal of Atmospheric and Solar-Terrestrial Physics*. 2001;63(5):441-9.
- [2] Baumjohann W, Blanc M, Fedorov A, Glassmeier KH. Current systems in planetary magnetospheres and ionospheres. *Space science reviews*. 2010;152:99-134.
- [3] Mayr H, Volland H. Magnetic storm characteristics of the thermosphere. *Journal of Geophysical Research*. 1973;78(13):2251-64.
- [4] Prolss G. Ionospheric F-region storms. *Handbook of atmospheric electrodynamics*, edited by: Volland, H. CRC Press; 1995.
- [5] Schunk RW, Sojka JJ. Ionosphere-thermosphere space weather issues. *Journal of Atmospheric and Terrestrial Physics*. 1996;58(14):1527-74.
- [6] Buonsanto MJ. Ionospheric storms—A review. *Space Science Reviews*. 1999;88(3-4):563-601.
- [7] Schunk R, Nagy A. *Ionospheres: physics, plasma physics, and chemistry*. Cambridge university press; 2009.

- [8] Mendillo M. Storms in the ionosphere: Patterns and processes for total electron content. *Reviews of Geophysics*. 2006;44(4).
- [9] Dahal S, Adhikari B, Khadka AK, Silwal A, Gupta SK, Chapagain NP. Ionospheric signatures during G2, G3 and G4 storms in mid-latitude. *Radio Science*. 2022;57(5):1-22.
- [10] Pirog O, Polekh N, Tashchilin A, Romanova E, Zherebtsov G. Response of ionosphere to the great geomagnetic storm of September 1998: Observation and modeling. *Advances in Space Research*. 2006;37(5):1081-7.
- [11] Balan N, Alleyne H, Otsuka Y, Vijaya Lekshmi D, Fejer B, McCreia I. Relative effects of electric field and neutral wind on positive ionospheric storms. *Earth, planets and space*. 2009;61(4):439-45.
- [12] Balan N, Shiokawa K, Otsuka Y, Kikuchi T, Vijaya Lekshmi D, Kawamura S, et al. A physical mechanism of positive ionospheric storms at low latitudes and midlatitudes. *Journal of Geophysical Research: Space Physics*. 2010;115(A2).
- [13] Huba J, Joyce G, Fedder J. Sami2 is Another Model of the Ionosphere (SAMI2): A new low-latitude ionosphere model. *Journal of Geophysical Research: Space Physics*. 2000;105(A10):23035-53.
- [14] Pavlov A, Pavlova N. Comparison of modeled electron densities and electron and ion temperatures with Arecibo observations during undisturbed and geomagnetic storm periods of 7–11 September 2005. *Journal of Geophysical Research: Space Physics*. 2011;116(A3).
- [15] Sojka JJ, Schunk RW, Denig W. Ionospheric response to the sustained high geomagnetic activity during the March'89 great storm. *Journal of Geophysical Research: Space Physics*. 1994;99(A11):21341-52.
- [16] Namgaladze A, Förster M, Yurik RY. Analysis of the positive ionospheric response to a moderate geomagnetic storm using a global numerical model. In: *Annales Geophysicae*. vol. 18. Springer Verlag Göttingen, Germany; 2000. p. 461-77.
- [17] Lei J, Wang W, Burns AG, Solomon SC, Richmond AD, Wiltberger M, et al. Observations and simulations of the ionospheric and thermospheric response to the December 2006 geomagnetic storm: Initial phase. *Journal of Geophysical Research: Space Physics*. 2008;113(A1).
- [18] Pawlowski DJ, Ridley AJ, Kim I, Bernstein DS. Global model comparison with Millstone Hill during September 2005. *Journal of Geophysical Research: Space Physics*. 2008;113(A1).
- [19] Klimenko M, Klimenko V, Ratovsky K, Goncharenko L. Ionospheric effects caused by the series of geomagnetic storms of September 9-14, 2005. *Geomagnetism & Aeronomy*;51(3):364-76.
- [20] Rishbeth H, Garriott OK. *Introduction to ionosphere physics*. Academic Press; 1969.
- [21] Gonzalez WD, Tsurutani BT, Clúa de Gonzalez AL. Interplanetary origin of geomagnetic storms. *Space Science Reviews*. 1999;88(3-4):529-62.
- [22] Dessler A, Parker EN. Hydromagnetic theory of geomagnetic storms. *Journal of Geophysical Research*. 1959;64(12):2239-52.
- [23] Skopke N. A general relation between the energy of trapped particles and the disturbance field near the Earth. *Journal of Geophysical Research*. 1966;71(13):3125-30.

- [24] Dungey JW. Interplanetary magnetic field and the auroral zones. *Physical Review Letters*. 1961;6(2):47.
- [25] Gonzalez W, Joselyn JA, Kamide Y, Kroehl HW, Rostoker G, Tsurutani B, et al. What is a geomagnetic storm? *Journal of Geophysical Research: Space Physics*. 1994;99(A4):5771-92.
- [26] Adhikari B, Dahal S, Karki M, Mishra RK, Dahal RK, Sasmal S, et al. Application of wavelet for seismic wave analysis in Kathmandu Valley after the 2015 Gorkha earthquake, Nepal. *Geoenvironmental Disasters*. 2020;7(1):1-16.
- [27] Torrence C, Compo GP. A practical guide to wavelet analysis. *Bulletin of the American Meteorological society*. 1998;79(1):61-78.
- [28] Grinsted A, Moore JC, Jevrejeva S. Application of the cross wavelet transform and wavelet coherence to geophysical time series. *Nonlinear processes in geophysics*. 2004;11(5/6):561-6.
- [29] Xiang Y, Gao Y, Shi J, Xu C. Consistency and analysis of ionospheric observables obtained from three precise point positioning models. *Journal of Geodesy*. 2019;93:1161-70.
- [30] Da Rosa A, Waldman H, Bendito J, Garriott O. Response of the ionospheric electron content to fluctuations in solar activity. *Journal of Atmospheric and Terrestrial Physics*. 1973;35(8):1429-42.
- [31] Maraun D, Kurths J. Cross wavelet analysis: significance testing and pitfalls. *Nonlinear Processes in Geophysics*. 2004;11(4):505-14.
- [32] Adhikari B, Sapkota N, Dahal S, Bhattarai B, Khanal K, Chapagain NP. Spectral characteristic of geomagnetically induced current during geomagnetic storms by wavelet techniques. *Journal of Atmospheric and Solar-Terrestrial Physics*. 2019;192:104777.
- [33] Atulkar R, Bhardwaj S, Khatarkar P, Bhawre P, Purohit P. Geomagnetic disturbances and its impact on ionospheric critical frequency (foF2) at high, mid and low latitude region. *American Journal of Astronomy and Astrophysics*. 2014;2(6):61-5.
- [34] Pandit D, Chapagain N, Adhikari B. Study of Ionospheric Variability during Super Substorms. *Journal of Nepal Physical Society*. 2020;6(2):74-84.